



This is a repository copy of *Breaking the GaN material limits with nanoscale vertical polarisation super junction structures: A simulation analysis.*

White Rose Research Online URL for this paper:
<http://eprints.whiterose.ac.uk/115934/>

Version: Accepted Version

Proceedings Paper:

Unni, V. and Narayanan, E.M.S. orcid.org/0000-0001-6832-1300 (2017) Breaking the GaN material limits with nanoscale vertical polarisation super junction structures: A simulation analysis. In: Japanese Journal of Applied Physics. 2016 International Conference on Solid State Devices and Materials (SSDM2016), 26/09/2016 - 29/09/2016, Tsukuba, Japan. Japan Society of Applied Physics .

<https://doi.org/10.7567/JJAP.56.04CG02>

Reuse

Unless indicated otherwise, fulltext items are protected by copyright with all rights reserved. The copyright exception in section 29 of the Copyright, Designs and Patents Act 1988 allows the making of a single copy solely for the purpose of non-commercial research or private study within the limits of fair dealing. The publisher or other rights-holder may allow further reproduction and re-use of this version - refer to the White Rose Research Online record for this item. Where records identify the publisher as the copyright holder, users can verify any specific terms of use on the publisher's website.

Takedown

If you consider content in White Rose Research Online to be in breach of UK law, please notify us by emailing eprints@whiterose.ac.uk including the URL of the record and the reason for the withdrawal request.



eprints@whiterose.ac.uk
<https://eprints.whiterose.ac.uk/>

Breaking the GaN Material Limits with Nanoscale Vertical Polarisation Super Junction Structures – A Simulation Analysis

Vineet Unni* and E.M. Sankara Narayanan

Department of Electronic and Electrical Engineering, University of Sheffield,

Wheeldon Street, Sheffield, S3 7HQ, United Kingdom

*E-mail: v.unni@sheffield.ac.uk

This is the first report on the numerical analysis of the performance of nanoscale vertical superjunction structures based on impurity doping and an innovative approach that utilizes the polarisation properties inherent in III-V nitride semiconductors. Such nanoscale vertical polarisation super junction structures can be realized by employing a combination of epitaxial growth along the non-polar crystallographic axes of Wurtzite GaN and nanolithography-based processing techniques. Detailed numerical simulations clearly highlight the limitations of a doping based approach and the advantages of the proposed solution for breaking the unipolar one-dimensional material limits of GaN by orders of magnitude.

1 INTRODUCTION

Gallium Nitride (GaN) power semiconductor devices are emerging as the chosen candidates for the next generation power electronic applications due to its superior intrinsic material properties in comparison to Silicon (Si). Present GaN power devices are of lateral topology. These structures utilize the high density and mobility of electrons that arise due to its polarisation properties (oriented along the c-axis), to achieve remarkable on-state conduction characteristics ^[1,2]. However, with the commercial availability of large area bulk GaN substrates with low dislocation density, development activities towards vertical devices are also gaining substantial traction ^[3-6]. Advantages of a vertical architecture include ease of voltage scalability, avalanche capability, enhanced reliability and reduction in specific on-state resistance ($R_{ON.A}$). However, the cost-performance ratio is limited for conventional vertical GaN devices as bulk GaN substrates remain expensive, and offer marginal gains over 4H-Silicon Carbide (SiC), which at present is considered a more mature wide bandgap device technology. Fig.1 shows the calculated one-dimensional material limits in terms of the variation in specific on-state resistance ($R_{ON.A}$) with breakdown voltage for GaN and 4H-SiC with reported data on vertical GaN devices from Avogy, Inc. To realize device performance beyond the material limits necessitates the use of superjunction (SJ) concept or conductivity modulation.

SJ structures in Si operate on the principle of charge balance in precisely doped alternating p-type and n-type columns ^[7-9]. Li et al. have previously reported on the design, simulations and optimisation of 5-20kV GaN and SiC vertical superjunction structures ^[10]. The optimisation in that simulation study was performed by

varying the pillar dosage, length and width (1 μm – 8 μm), and it was observed that a reduction in the specific on-state resistance ($R_{\text{ON,A}}$) by more than one order of magnitude was observed only when the breakdown voltage was in the range of 10kV, while employing pillar widths of 1-3 μm . It also needs to be recognized that dopant based approach in GaN is very immature and is unrealistic due to difficulties of controlled Mg activation ^[11]. However, this challenge has been overcome by realizing superjunction structures in lateral GaN devices using polarisation engineering ^[12-19].

With the availability of polar and non-polar bulk GaN substrates and the advances that have been made recently in the growth/over-growth of high aspect ratio GaN nano-columns ^[20-22], a highly innovative solution using the intrinsic polarisation properties of GaN has been proposed and discussed herein. Performance analysis of vertical GaN power semiconductor devices based on conventional SJ as well as vertical polarisation super junction (VIP-SJ) concepts are presented. The analysis shows that by adopting the new approach, the limited cost-performance ratio of conventional vertical GaN solutions can be significantly improved and render this technology to be highly competitive for the next generation of power electronic applications.

2 VERTICAL POLARISATION SUPER JUNCTION

Non-polar GaN is currently being widely pursued/investigated for optoelectronic applications, and there is an existing global supply chain for non-polar GaN template-based epitaxy as well as native substrates. By growing Wurtzite GaN along non-polar axes, the orientation of the intrinsic polarisation can be controlled to be directed laterally in the grown layers. This single aspect forms the fundamental basis for realizing VIP-SJ

structures.

Fig. 2 shows the schematic of a conceptual GaN-AlGaN-GaN VIP-SJ structure grown along a non-polar axis (perpendicular to the polar c-axis). It also illustrates the inherent compensation of polarisation charges and accumulation of high density/mobility charge carriers (two-dimensional electron gas (2DEG)/two-dimensional hole gas (2DHG)). As in a lateral PSJ device, the on-state conduction can take place primarily using the 2DEG which is both doping and temperature independent. During off-state, the polarisation charges along the GaN(0001)/AlGaN(000 $\bar{1}$) and AlGaN(0001)/GaN(000 $\bar{1}$) vertical interfaces compensate each other, enabling a uniform ‘box’ like electric field distribution. This maximizes the breakdown voltage for a given drift thickness ^[12-17].

3 NUMERICAL SIMULATION

Numerical two-dimensional device simulations were performed using Silvaco ATLAS. The following models were included: FERMI, SRH, SELB, FMCT.P and FMCT.N. An optimal charge density of $1 \times 10^{13} \text{ cm}^{-2}$ was assumed for both the doped and VIP-SJ structures. For a doped SJ structure, the doping density in the p and n columns was derived and set as $2.05 \times 10^{17} \text{ cm}^{-3}$ and $2.05 \times 10^{18} \text{ cm}^{-3}$ for effective pillar widths of 1 μm and 100 nm respectively ^[23]. For the VIP-SJ structures, interface charge density of $+1 \times 10^{13} \text{ cm}^{-2}$ and $-1 \times 10^{13} \text{ cm}^{-2}$ was defined at the alternating interfaces. The doping concentration in the N+ region was set as $1 \times 10^{19} \text{ cm}^{-3}$. The simulated structures (Schottky Barrier Diodes) with a pillar width of 100 nm have been shown in Figs. 3 (a)-(b), and the energy band diagram also depicting the carrier concentration within the VIP-SJ structure has been shown in Fig. 3 (c). In this article, detailed results and comparison of the

performance between the two types of superjunction structures have been presented for those with pillar width of 100 nm; utilizing such nanoscale structures can yield unprecedented improvement in performance of vertical GaN devices.

3.1 Breakdown Characteristics:

In order to simulate avalanche breakdown, the Selberherr impact ionization-generation model was activated in the program. Default impact ionization parameters for GaN as defined in Silvaco ATLAS manual were used in this study ^[24].

Reverse I-V characteristics and the electric field profile within the simulated structures for different drift thicknesses (shown in parentheses in the charts) and accordingly at various reverse bias conditions (just before occurrence of avalanche breakdown) have been shown in Figs. 4 (a) – (b) respectively. The simulated values for breakdown voltage were comparable between the two types of device structures. Verification of the electric field distribution within both VIP-SJ and doped SJ structures indicated uniformity within the bulk of the drift region, as expected under ideal charge-balance conditions.

3.2 On-State Characteristics:

For superjunction structures based on doping, the doping concentration of the drift region is primarily dictated by the cell pitch ^[23]. Therefore, by reducing the cell pitch, the doping density in the pillars can be increased to obtain lower specific on-state resistance for a given breakdown voltage under ideal charge-balance conditions.

In the simulation, the workfunction to obtain a Schottky contact between the Anode electrode and N-type GaN region was set as 5.3 eV in both doped as well as VIP-SJ structures. In the VIP-SJ structure, Anode

makes a Schottky contact to the 2DEG that forms along the vertical GaN(0001)/AlGaN(000 $\bar{1}$) interface. An ideal Ohmic contact has been assumed to the P-type GaN region and 2DHG in the doped and VIP-SJ structures respectively. Forward I-V characteristics of the simulated structures for different drift thicknesses have been shown in Fig. 5. As shown, the on-set voltage is $\sim 0.8\text{V}$ in all the structures. However, the anode current density obtained in the PSJ structures is almost three times higher when compared to the doped SJ structures. There are two fundamental reasons behind the observed differences, which have been described below:

- i. Reduced mobility with high doping concentration: On-state conduction in the doped SJ structures takes place in the N-type pillar regions. At higher doping concentrations, electron mobility deteriorates due to increased ionized impurity scattering with the ionized doping atoms. This aspect has been clearly captured in Fig. 6, where a correlation between electron mobility and donor density has been plotted for Si, 4H-SiC and GaN ^[26-28]. In the case of VIP-SJ devices, no such deterioration in mobility occurs due to structure being undoped.
- ii. Ineffective utilization of the cell active area: The total current density in the two types of superjunction structures has been depicted in Figs. 7 (a) – (b). As shown in Fig. 7 (a), the active area utilization in a doped structure is limited due to lateral depletion that occurs even under thermal equilibrium conditions. With reduced effective active area for conduction, the specific on-state resistance doesn't decrease significantly with pitch. For PSJ transistors, no change in the effective active area for conduction occurs with a reduction in pitch, as the current flow is determined purely by the high

density/mobility 2DEG.

The overall scenario comparing theoretical material limits and results from the simulation have been summarized in Fig. 8. As shown in the figure, compared to the material limits, a reduction of almost two orders of magnitude in R_{ON-A} can be achieved using VIP-SJ structures for breakdown voltage of 1kV, which could extend to an improvement by three orders of magnitude for 10kV devices, in comparison to conventional 4H-SiC devices.

4 CONCLUDING REMARKS

GaN Superjunction structures with a pillar-width of 100 nm require doping concentration in the range of 10^{18} cm^{-3} . With activation ratio of 1% at 300K using Mg as the dopant, p-type doping remains as one of the key challenges in GaN device processing. Temperature dependent activation of p-type doping will limit the temperature range over which charge-balance can be maintained in such structures. The increased doping density that's accompanied by a reduction in pitch leads to significant degradation of electron mobility, leading to diminishing improvement in the specific on-state resistance (R_{ON-A}) with increased N-type doping density. This in combination with lateral depletion even under thermal equilibrium causes ineffective utilization of the active area and leads to sub-optimal performance of such doping-based superjunction structures. Vertical PSJ structures overcome the above-mentioned challenges as on-state conduction takes place using high density/mobility 2DEG, maintaining temperature-independent charge balance under off-state conditions. Compared to the material limits, a reduction of almost two orders of magnitude in R_{ON-A} can be achieved using PSJ structures for breakdown voltage of 1kV, which could extend to three orders of

magnitude improvement for 10kV devices, in comparison to 4H-SiC. In conclusion, the proposed polarisation engineering is an effective and viable solution to realize ultra-high efficient vertical GaN power semiconductor devices. Apart from the potential of dramatically improving energy savings, this will also pave the path towards a truly competitive wide bandgap technology for wider acceptance by the market.

ACKNOWLEDGMENTS

Vineet Unni acknowledges the support of EPSRC Doctoral Prize Fellowship provided by EPSRC and the University of Sheffield for undertaking this work.

Reference list

- [1] M. A. Khan, J. N. Kuznia, J. M. Van Hove, N. Pan, and J. Carter, *Appl. Phys. Lett.* **60**, 3027 (1992).
- [2] O. Ambacher, J. Smart, J. R. Shealy, N. G. Weimann, K. Chu, M. Murphy, W. J. Schaff, L. F. Eastman, R. Dimitrov, L. Wittmer, M. Stutzmann, W. Rieger, and J. Hilsenbeck, *J. Appl. Phys.* **85**, 3222 (1999).
- [3] I. C. Kizilyalli, A. P. Edwards, H. Nie, D. Bour, T. Prunty, and Don Disney, *IEEE Electron Device Lett.*, **35**, 247 (2014).
- [4] H. Ohta, N. Kaneda, F. Horikiri, Y. Narita, T. Yoshida, T. Mishima, and T. Nakamura, *IEEE Electron Device Lett.*, **36**, 1180 (2015).
- [5] T. Oka, T. Ina, Y. Ueno, and J. Nishii, *Proc. Int. Symp. Power Semiconductor Devices and ICs*, 2016, p. 459.
- [6] K. Nomoto, B. Song, Z. Hu, M. Zhu, M. Qi, N. Kaneda, T. Mishima, T. Nakamura, D. Jena, and H. G. Xing, *IEEE Electron Device Lett.* **37**, 161 (2016).
- [7] D. J. Coe, US Patent # 4754310 (1988).
- [8] T. Fujihira, *Jpn. J. Appl. Phys.* **36**, 6254 (1997).
- [9] G. Deboy, M. Marz, J. P. Stengel, H. Strack, J. Tihanyi, and H. Weber, *Proc. Int. Electron Devices Meeting*, 1998, p. 683.
- [10] Z. Li, H. Naik, and T. P. Chow, *Proc. Lester Eastman Conference on High Performance Devices*, 2012, p. 1.
- [11] U. Kaufmann, P. Schlotter, H. Obloh, K. Kohler, and M. Maier, *Phys. Rev. B*, **62**, 10867 (2000).

- [12] A. Nakajima, K. Adachi, M. Shimizu, and H. Okumura, *Appl. Phys. Lett.* **89**, 193501-1 (2006).
- [13] A. Nakajima, Y. Sumida, M. H. Dhyani, H. Kawai, and E. M. S. Narayanan, *Appl. Phys. Express.* **3**, 121004-1 (2010).
- [14] A. Nakajima, Y. Sumida, M. H. Dhyani, H. Kawai, and E. M. S. Narayanan, *IEEE Electron Device Lett.* **32**, 542 (2011).
- [15] A. Nakajima, M. H. Dhyani, Y. Sumida, H. Kawai, and E. M. S. Narayanan, *Proc. Int. Symp. Power Semiconductor Devices and ICs*, 2011, p. 280.
- [16] A. Nakajima, V. Unni, K. G. Menon, M. H. Dhyani, Y. Sumida, H. Kawai, and E. M. S. Narayanan, *Proc. Int. Symp. Power Semiconductor Devices and ICs*, 2012, p. 265.
- [17] V. Unni, H. Long, M. Sweet, A. Balachandran, A. Nakajima, H. Kawai, and E. M. S. Narayanan, *Proc. Int. Symp. Power Semiconductor Devices and ICs*, 2014, p. 245.
- [18] V. Unni, and E. M. S. Narayanan, *Proc. Wide Bandgap Semiconductor and Components Workshop*, 2016.
- [19] V. Unni, and E. M. S. Narayanan, *Proc. International Seminar on Power Semiconductors*, 2016.
- [20] K. Xing, Dr. Thesis, Faculty of Engineering, University of Sheffield, Sheffield (2015).
- [21] E.D. Le Boulbar, C.J. Lewins, D.W.E. Allsopp, C.R. Bowen, and P.A. Shields, *Microelectron. Eng.* **153**, 132 (2016).
- [22] S. Y. Bae, B. O. Jung, K. Lekhal, S. Y. Kim, J. Y. Lee, D. S. Lee, M. Deki, Y. Honda, and H. Amano, *Cryst. Eng. Comm.* **18**, 1505 (2016).

- [23] B. J. Baliga, *Fundamentals of Power Semiconductor Devices*, (Springer, New York, 2008), p. 16.
- [24] *ATLAS User's Manual*, Silvaco, Santa Clara, California, USA.
- [25] M. Ishida, M. Kuroda, T. Ueda, and T. Tanaka, *Semicond. Sci. Technol.* **27** 024019 (2012).
- [26] N. G. Wright, D. J. Morrison, C. M. Johnson, and A. G. O'Neill, *Mater. Sci. Forum*, **264–268**, 917 (1998).
- [27] T. T. Mnatsakanov, M. E. Levinshtein, L. I. Pomortseva, S. N. Yurkov, G. S. Simin, and M. A. Khan, *Solid-State Electron.* **47**, 111 (2003).
- [28] A. Nakajima, M. Shimizu, and H. Ohashi, *IEEE Trans. Electron Devices*, **56**, 2652 (2009).

Figure Captions:

Figure 1: Calculated variation in specific on-state resistance with breakdown voltage (one dimensional material limits).

Figure 2: Schematic illustration of atomic arrangement in a vertical GaN-AlGaN-GaN PSJ structure (adapted from ^[25]).

Figure 3: Simulated structures (pillar-width=100 nm) (a) Doped SJ (b) VIP-SJ (c) Energy band diagram (VIP-SJ, along the dashed line at thermal equilibrium).

Figure 4: Simulated (a) Breakdown characteristics (b) Electric field profile plotted vertically along the high field drift region (Anode to Cathode), at various reverse bias conditions.

Figure 5: Forward I-V characteristics (pillar-width=100 nm).

Figure 6: Electron mobility as a function of doping density ^[26-28].

Figure 7: Distribution of total current density at $V_{AC}=3V$ (a) Doped SJ (b) VIP-SJ.

Figure 8: Calculated variation in specific on-state resistance with breakdown voltage, including the one-dimensional superjunction limits and simulation results.

Figure 1:

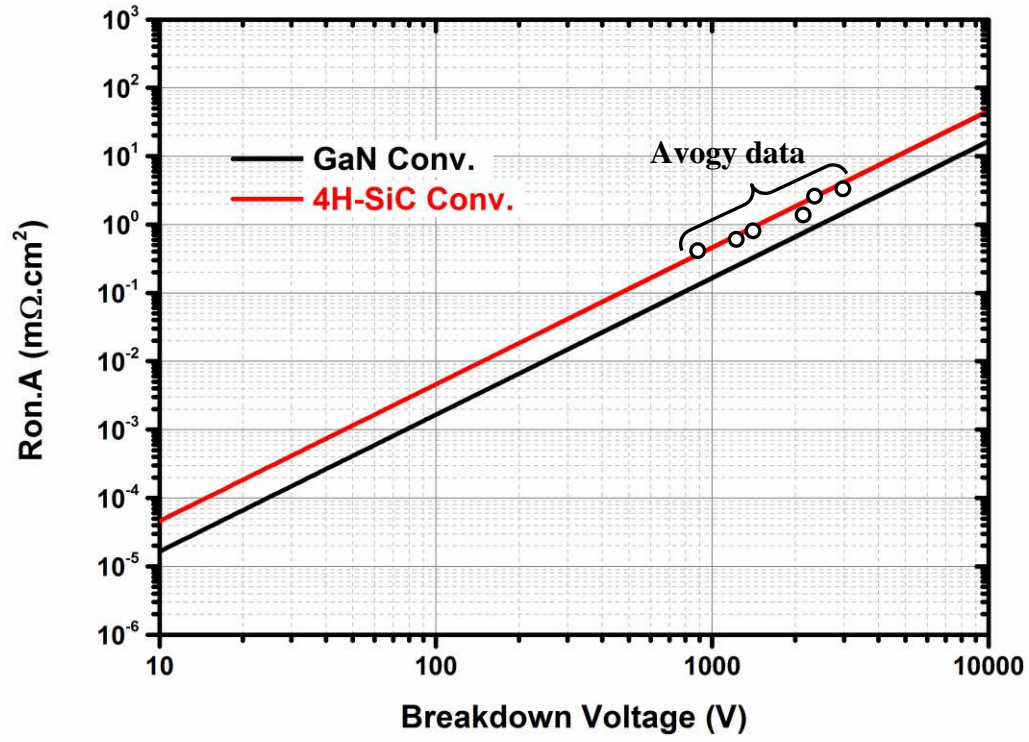


Figure 3:

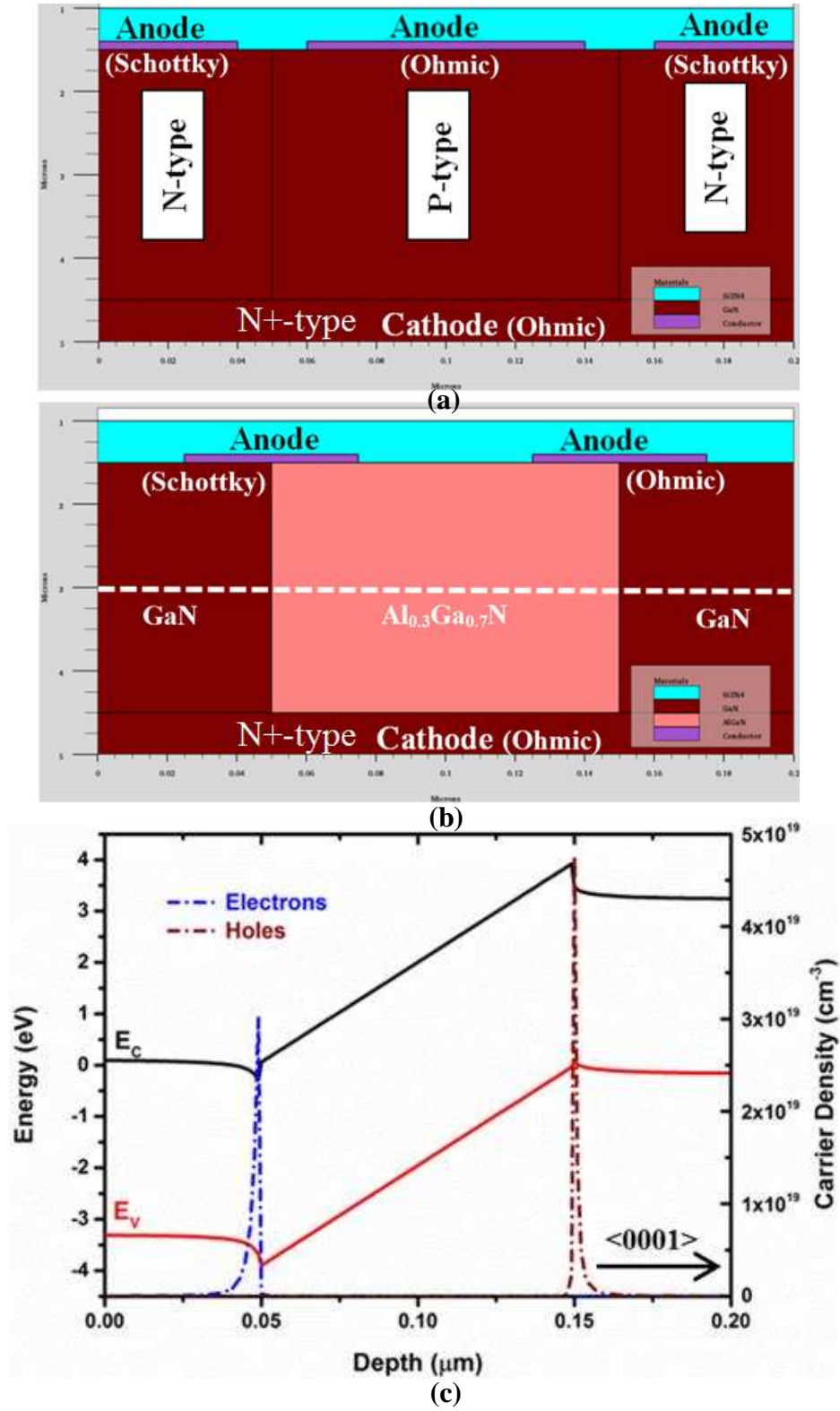
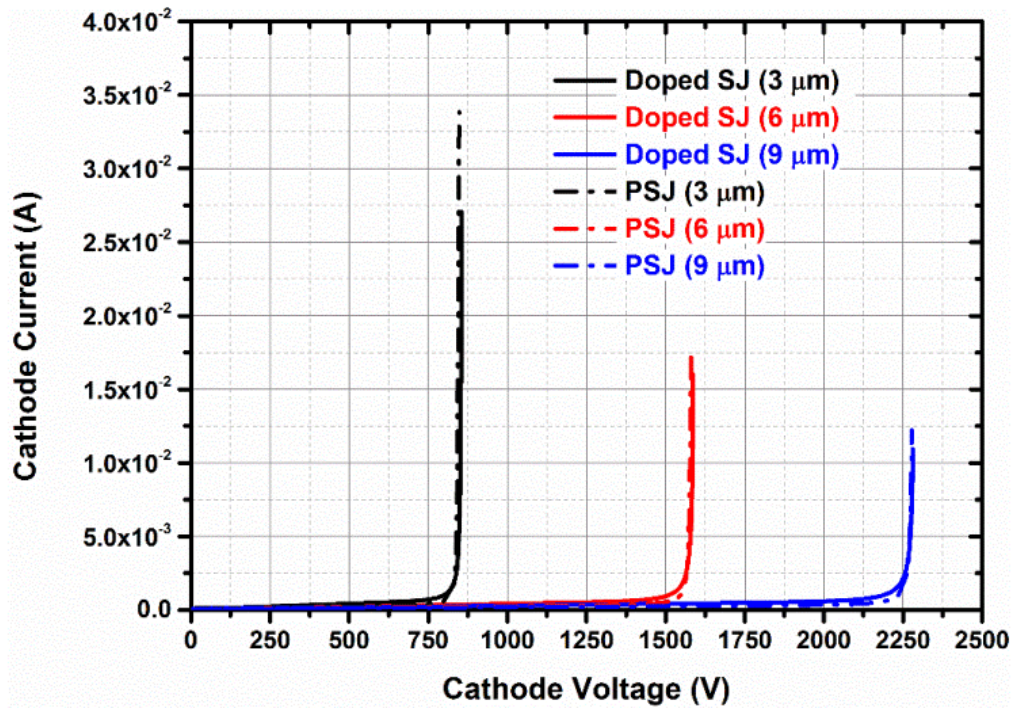
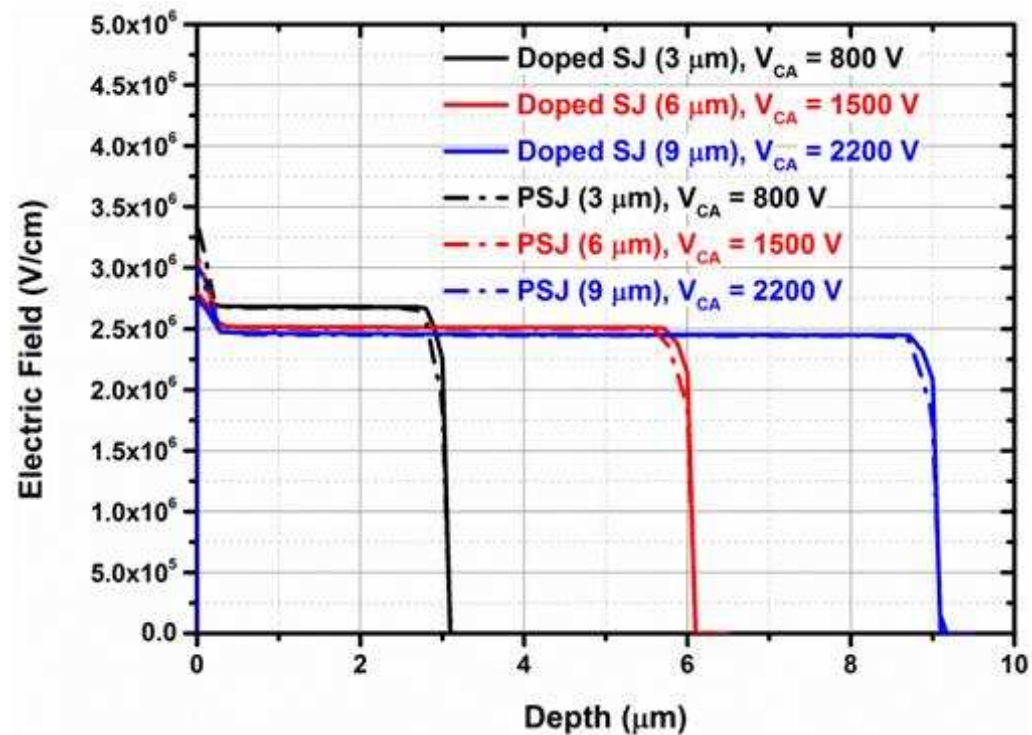


Figure 4:



(a)



(b)

Figure 5:

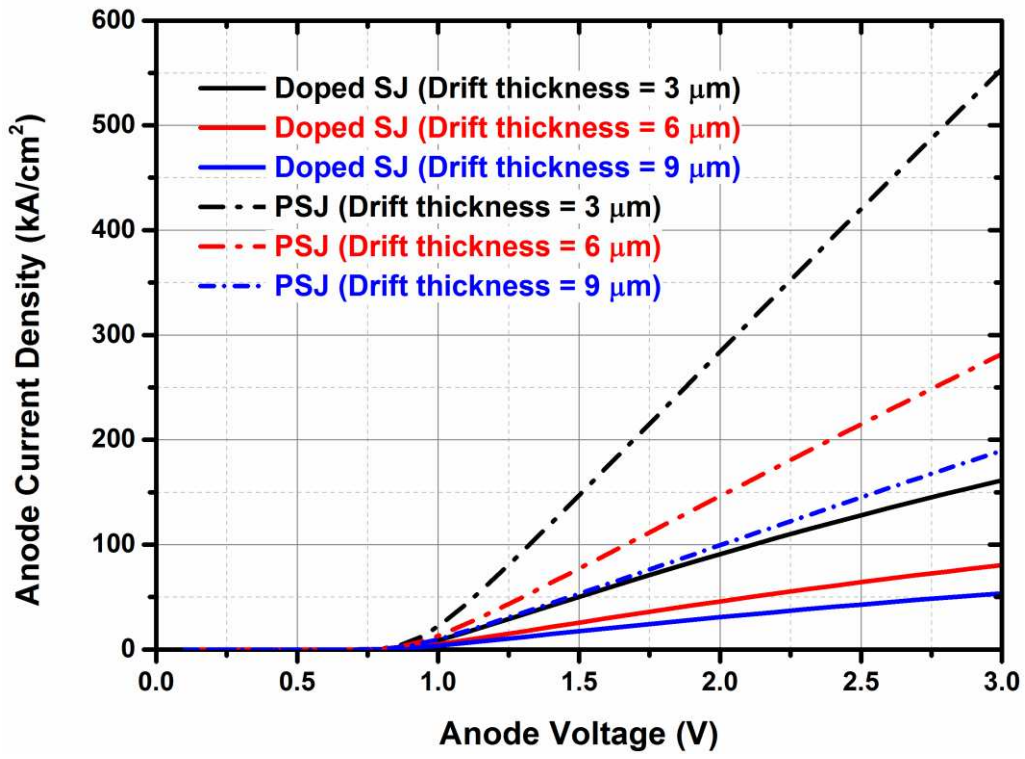


Figure 6:

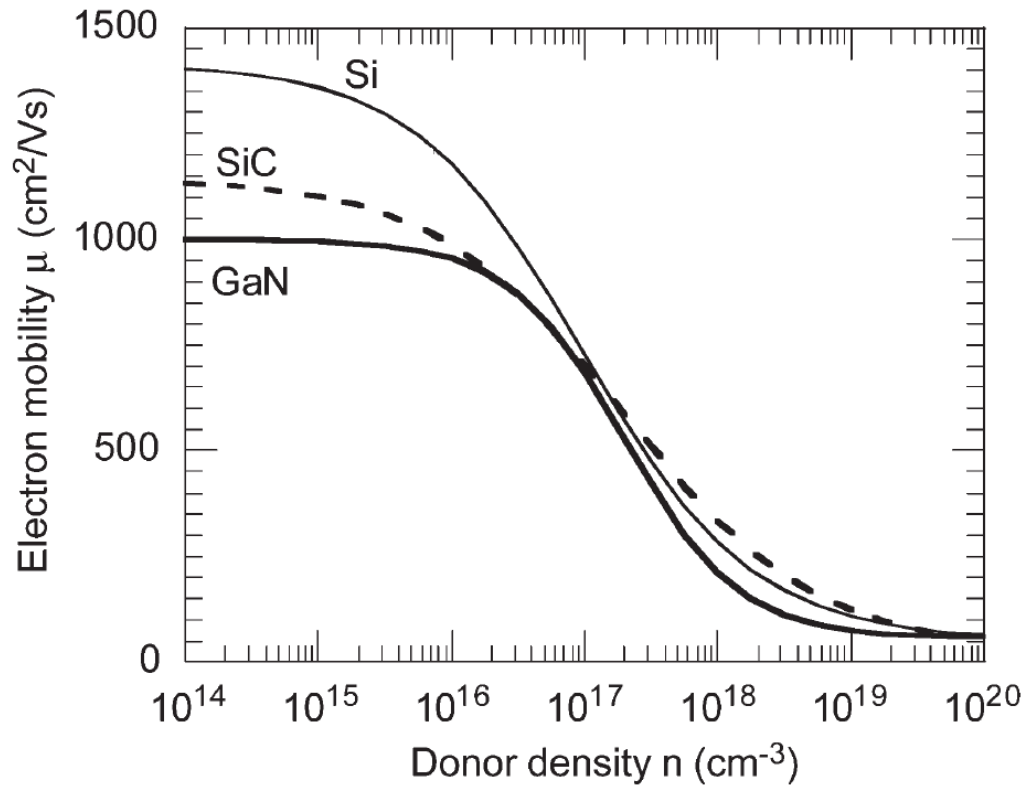


Figure 7:

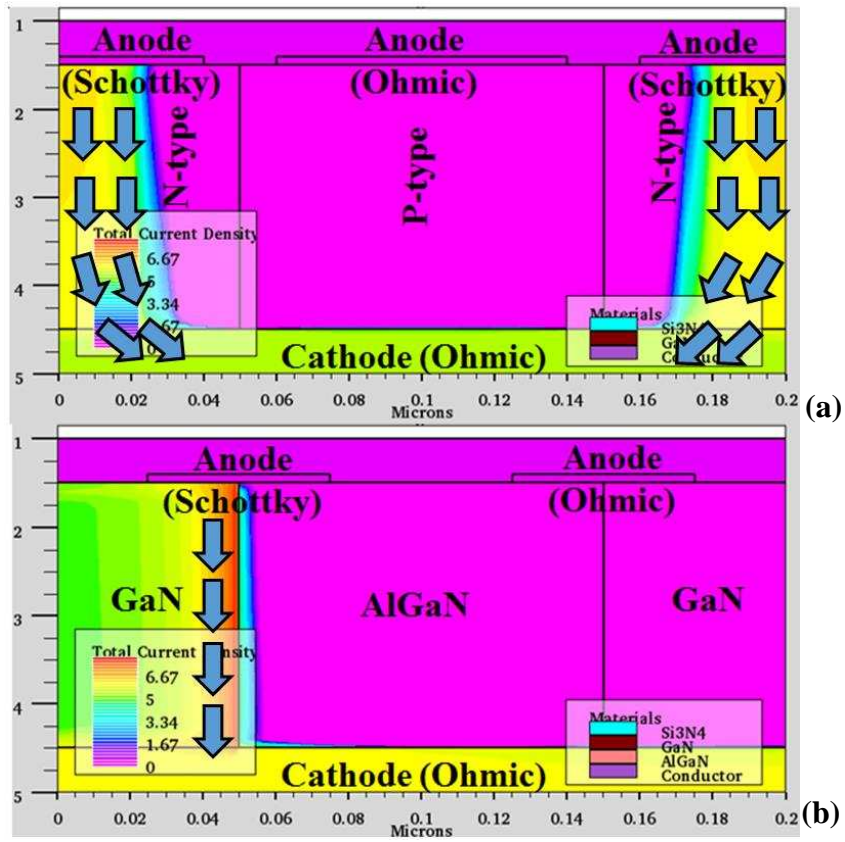


Figure 8:

